



Study on the characteristics of hydrogen bubble formation and its transport during electrolysis of water

Prasad Chandran, Shamit Bakshi*, Dhiman Chatterjee

Department of Mechanical Engineering, Indian Institute of Technology Madras, Chennai 600036, India



HIGHLIGHTS

- Hydrogen bubble formation and its transport near the electrode surface during electrolysis.
- Mean bubble size near the cathode decreases continuously before reaching a steady state for high current density.
- Bubble size distribution changes from bi-modal to log-normal with passage of time.
- Bubble growth rate and the velocities strongly influence the near-electrode bubble size distribution.

ARTICLE INFO

Article history:

Received 16 May 2015

Received in revised form

21 July 2015

Accepted 26 July 2015

Available online 10 August 2015

Keywords:

Bubble size distribution

Hydrogen bubble

Bubble growth

Electrolysis

ABSTRACT

This study experimentally investigates the characteristics of hydrogen bubble formation and its transport near the electrode surface during the electrolysis of water. It is observed that the mean size of the bubble and its distribution near the cathode continuously changes over a period of an hour before reaching a steady state, particularly for high superficial current density (1200 mA/cm^2). The reason for this variation is explained using temporal evolution of the measured velocity distribution of bubbles having different sizes. A bubble plume constitutes of several individual bubble streams interacting with each other. The growth of the big bubbles on the electrode surface and the small bubbles along the stream follows diffusion laws of growth in a solution supersaturated with hydrogen. It is shown that this growth rate along with the detached bubble velocity is vital in determining the bubble size distribution near the electrode surface.

© 2015 Elsevier Ltd. All rights reserved.

1. Introduction

Bubble formation in electrolysis of water is a widely observed process in the gas evolving electrodes of different practical applications like electroplating, electrowinning, hydrogen production (Nierhaus et al., 2009; Zeng and Zhang, 2010). This process is also recently gaining importance in various finer techniques like delamination of graphene (Wang et al., 2011) or making of microfilms (Plowman et al., 2015). Many of these applications (Nierhaus et al., 2009; Zeng and Zhang, 2010) are presently being studied more carefully with a view to accurately simulate the process which can aid in improving them (Nierhaus et al., 2009; Jomard et al., 2008; Charton et al., 2010). The complexity in the gas evolution process poses additional modelling difficulties apart from that of simulating two-phase flow. Electrolysis of water produces hydrogen bubbles with size distribution depending on different factors. The water near the cathode gets supersaturated

(Kikuchi et al., 2006) with hydrogen and hence the release of hydrogen at the electrode nucleates bubble at the electrode surface at several nucleation sites. The bubble then grows and eventually detaches from the surface of the electrode as the detaching forces supersede the surface tension force. The bubbles may keep growing even after detachment from the cathode surface as long as the surrounding liquid remains supersaturated. The bubble formation contributes significantly to electrode overpotential and the actual current density is much higher than the superficial or nominal current density. This has been quite well studied in literature and empirical as well as theoretical relations exist for the same (Vogt and Balzer, 2005; Vogt, 2012). The bubble coverage is an important parameter in this context which is the fraction of the total electrode area rendered inactive due to bubble formation. It has been shown recently (Vogt, 2012) that bubble coverage exhibit complex dependence on different parameters like the gas flow rate, residence time of the bubbles and bubble volume at departure from the electrode amongst other things. A sole dependence of bubble coverage on nominal current densities can result in unrealistic values at higher bubble coverages. In a more recent study (Vogt and Stephan, 2015), the details of the

* Corresponding author.

E-mail address: shamit@iitm.ac.in (S. Bakshi).

local microprocesses are considered to obtain better description of mass transfer at gas-evolving electrodes. It will be useful to see the effect of considering bubble size distribution on mass transfer using this analysis. Hence, it is apparent that the bubble size distribution on the electrode surface and its characteristics will be of significance to the literature.

The bubble size distribution can serve as a vital input to the computational efforts for accurately simulating electrolytic processes involving gas evolution. The techniques used in most of the work on electrolysis bubble computations uses a mono-disperse bubble size on the electrode surface (Jomard et al., 2008; Charton et al., 2010). There have been efforts as well to prescribe the measured bubble size distribution at the electrode surface in computer simulations (Nierhaus et al., 2009; Murai and Matsumoto, 2000). However, the characteristics of bubble size distribution on electrode surface could be quite complex. For example, Vogt and Balzer (Vogt and Balzer, 2005) reported a change in bubble coverage with passage of time after the starting of electrolysis. It is of interest to see if this change in coverage changes the bubble size distribution and the mean bubble size. The growth of bubbles on the electrode surface is of interest and has been experimentally investigated (photographically) from an early time (Westerheide and Westwater, 1961). Janssen and Hoogland (Janssen and Hoogland, 1970, 1973) also studied the effect of the nature of gas evolved and current density on the number and distribution of nucleation sites. It would be further interesting to see the effect of the growth of bubbles near the electrode surface on the size distribution. However, there has been a very limited study on the characteristics of the size distribution on the electrode surface. The distribution could be quite useful in drawing important conclusions about the electrolysis process. For example, Khosla et al. (1991) in their work demonstrated the importance of pulsed electrolysis using bubble size distribution

measurements. Tanaka et al. (2005) on the other hand utilized bubble size distribution data to demonstrate the inhibition of bubble coalescence with the enhancement of electrolyte concentration. Lee et al. (2005) measured bubble size distribution from an electrolytic microbubbler and established a nearly monodisperse bubble size with an average diameter of 40 µm.

Keeping in view the literature above, the experimental results reported in this work attempts to develop a deeper insight into the process of electrolysis bubble formation and its transport and presents the critical processes involved therein. In the next section, the experimental setup and technique adopted to carry out this investigation is reported. This is followed by results and discussion and finally a summary of the major findings from this work.

2. Experimental setup and methodology

Fig. 1(a) shows the schematic of the experimental setup. The setup consists of test section which includes a tank with square base, an electrode arrangement, a DC power supply and an imaging system. The tank is made of acrylic with a base of 360 mm on each side and a height of 830 mm. The tank is filled with an electrolyte solution (5 mM aqueous solution of sodium chloride) up to a height of 300 mm from the cathode surface. All the experiments are conducted under atmospheric condition. The electrode arrangement (Fig. 1(b)) comprises of an anode made of copper clad laminate and a cathode made of copper sheet embedded in the acrylic holder. The cathode is a commercially available thin copper foil and is used as a bubble generator. To evaluate the purity of the cathode material, an EDAX analysis was performed which revealed that the electrode material used contains 97.56% by weight of copper. It is 125 mm long, 10 mm wide

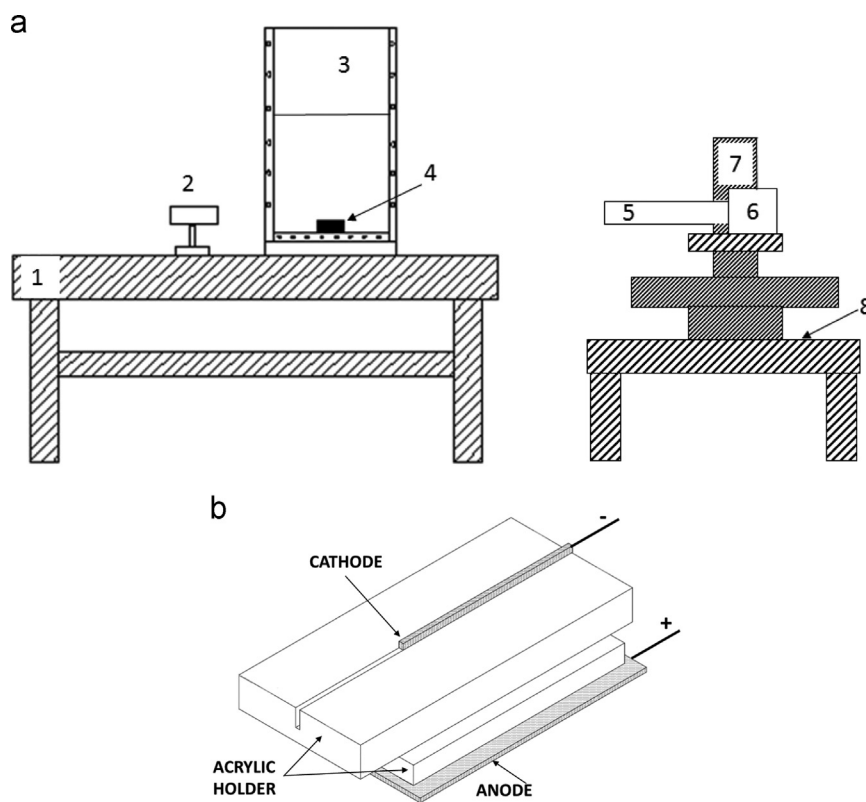


Fig. 1. (a) Schematic of experimental arrangement for bubble size and velocity measurements. (1) Optical table. (2) DC power supply. (3) LED strobe light. (4) Water tank (360 mm × 830 mm). (5) Electrode arrangement. (6) Long distance microscope. (7) XYZ traverse. (8) CCD camera. (9) Adjustable optical breadboard. (b) Schematic of electrode arrangement.

and 40 micron thick. The electrode strip is carefully cut out from the foil using a scissor and then washed and gripped tightly into a fine gap made on the acrylic electrode holder. Thus the two opposite surfaces and three edges of the strip remains covered and only one edge (40 micron) remain exposed to the electrolyte solution. This thin electrode facilitates the formation of a thin plume and a majority of the bubbles near the cathode remain in the plane passing through it. Thus, looking from a direction perpendicular to this plane, the bubbles remain within the depth of focus of the lens. It would be shown later that the mean size and distribution obtained are quite repeatable from different trials. The active edge of the cathode is placed horizontally to reduce the interaction of bubbles from different nucleation sites which otherwise can coalesce as they move upwards along the electrode surface. The anode is kept inverted to prevent the disturbance of the hydrogen bubble plume from the rising oxygen bubbles. Both the anode and cathode are flush mounted on the electrode holder. A DC power supply of 0–30 V, 0–5 A with a resolution of 10 mA is used to supply the voltage necessary for electrolysis. For measurement of bubble size in the plume a visualization system is used. This consists of a double shutter CCD camera, a LED strobe light, long distance microscope, synchronizing card and XYZ traverse controlled by microcontroller. The LED strobe light with minimum pulse width of 2 μ s is used as backlight for shadow imaging of bubbles in the bubble plume. The long distance microscope has a working distance of 560 mm to 1520 mm, and a resolution of 3 microns at 560 mm. This is used along with 2x Barlow lens for better magnification. The double shutter camera with a resolution of 1392 \times 1040 pixels is mounted on the XYZ traverse along with the long distance microscope to record the images of the bubbles. The camera has an interframing time of 2 ms and is also used for measuring the bubble velocity. A low frame rate is used in the double shutter camera to ensure that the bubbles captured in one frame do not reappear in the next and thereby provide statistically reliable data. The NI card (module 9401) is used as the trigger source for the double shutter camera and the strobe light for the purpose of synchronization. The experiments are performed for two different values of the currents namely 30 mA and 60 mA. Thus, the superficial current densities for the above-mentioned currents are 600 mA/cm² and 1200 mA/cm² respectively.

The planar view of a typical bubble plume, as produced by electrolysis in these experiments, is shown in the left of Fig. 2. The plume remains planar up to a certain height from the electrode surface and eventually transiting to a disturbed, three dimensional, dispersed structures. A magnified view, as seen using the long distance microscope, is seen in the right side of Fig. 2. Several bubble streams with different diameters rise from the electrode surface continuously.

The 8 bit grayscale images are processed by binarizing them using threshold intensity value. As the background can be non-uniform, a local threshold is used instead of a global threshold.

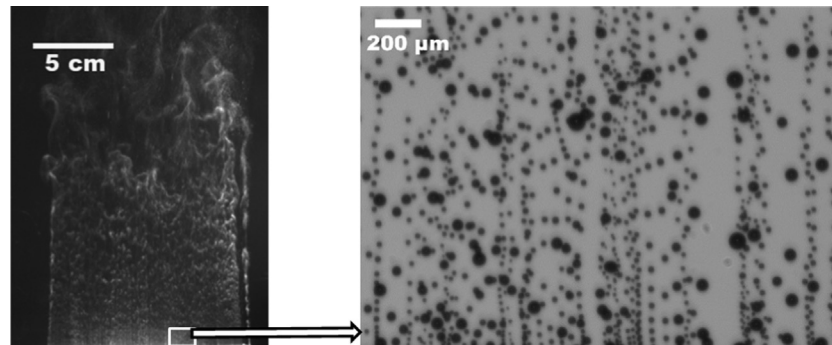


Fig. 2. Image on the left shows the planar view of the entire plume. Image on the right shows the magnified view of the plume originating from the electrode surface.

This local threshold for each pixel is obtained from the mean of intensity value within a small window. The window size is selected in such a way that the mean and standard deviation of the bubble diameter does not change significantly with a change in the window size. This elaborate technique was validated using some synthetic images created with known size distribution.

After binarizing the image, the bubbles are detected by identifying the connected components in the image using the image processing toolbox of Matlab[®]. The diameter of a bubble is calculated from the area of the labelled region. To avoid the detection of cluster of bubbles as a single bubble, the connected components above an eccentricity factor of 0.6 are excluded. Fig. 3 shows the detected bubbles for a typical image obtained using the above technique.

3. Results and discussion

3.1. Unsteady variation of the bubble size distribution from start of electrolysis

At first, we investigate the variation of bubble size distribution at different times from the beginning of the electrolysis process. This is in fact one important point to be presented in this paper. Fig. 4 presents the variation of the bubble size distribution with time. The left hand side of this figure shows typical magnified images of the bubble plume at a particular location on the electrode surface at a given time. The field of view of this image is 2.1 mm by 1.5 mm (width by height) with the bottom edge indicating the electrode surface. The right hand side shows the corresponding bubble size distribution. It should be noted that the distribution is obtained from several images captured (300 images) during this time and not just from the image on the left alone. The images on the left show that there are very few nucleation sites producing bubble streams to begin with and it gradually increases as time progresses. Although, with progress in

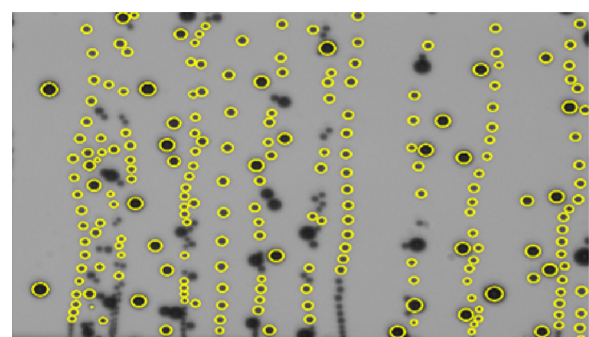


Fig. 3. Detected bubbles overlaid on the grayscale image.

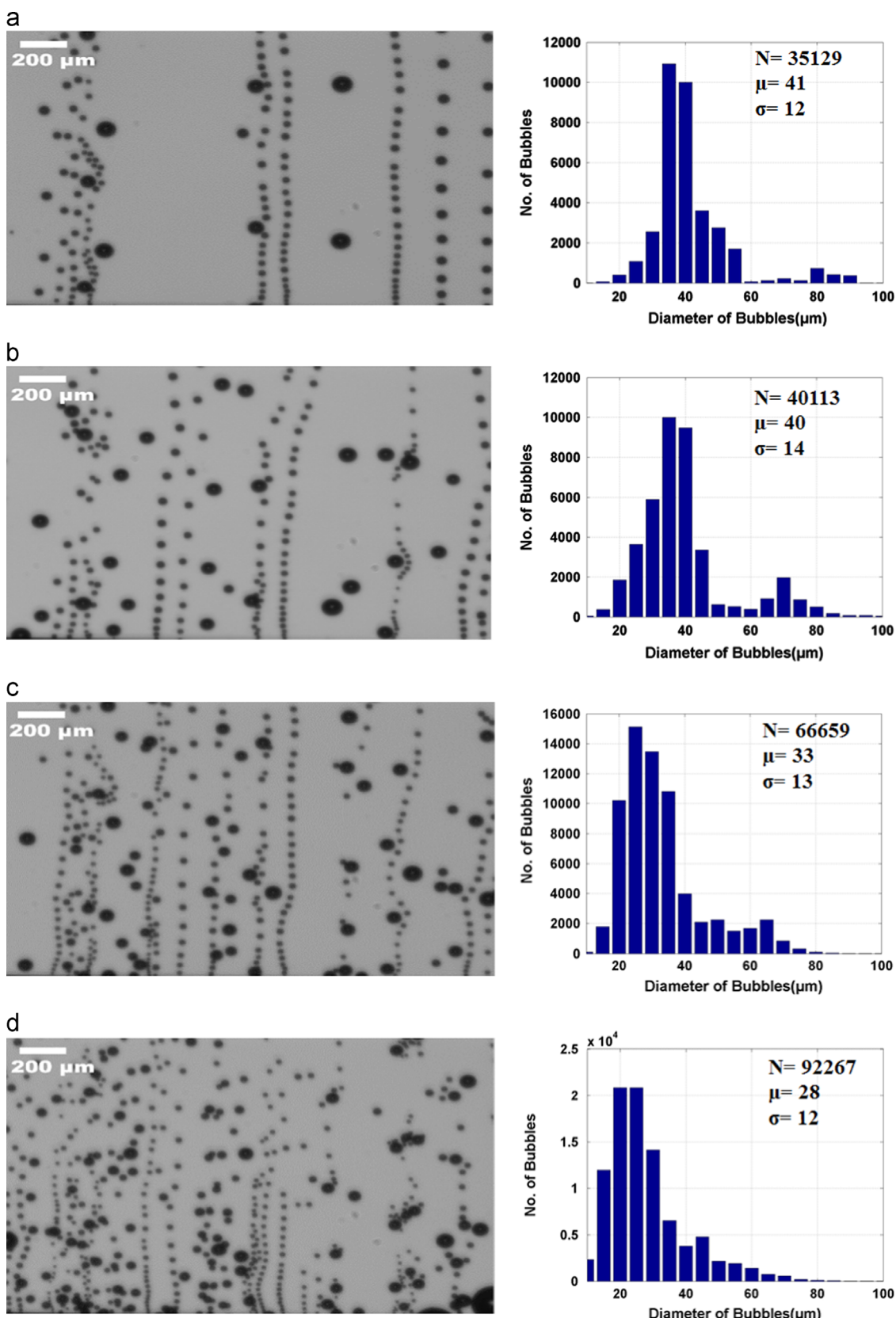
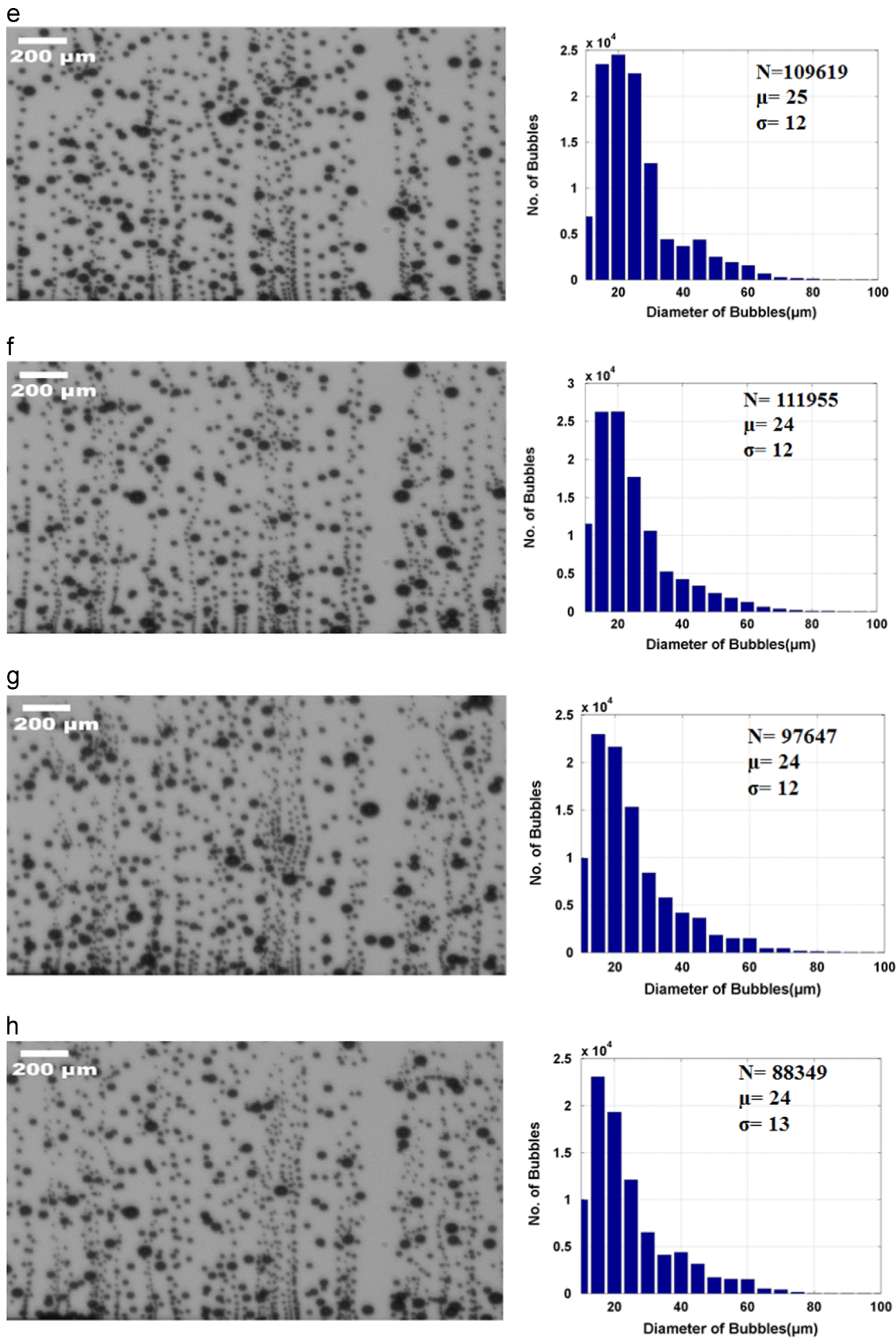


Fig. 4. The left side shows the instantaneous magnified image of the plume originating from the electrode surface and the right side shows the distribution of the bubble size. Current is 60 mA. The instant of time for these images are (a) $t=5$ min. (b) $t=12$ min. (c) $t=26$ min. (d) $t=40$ min. (e) $t=54$ min. (f) $t=68$ min. (g) $t=82$ min. (h) $t=96$ min. μ is the mean of the bubble size distribution, σ is the standard deviation of the bubble size distribution, N is the number of bubbles used for the distribution.

**Fig. 4. (continued)**

time, the interactions between the streams make it difficult to identify individual stream of bubbles, it is clear that the plume constitutes of a collection of several bubble streams interacting

with each other. The interactions can lead to clustering and coalescence of the bubbles. It can be noted that it almost takes an hour to reach close to a steady state. Few images indicating the

change in bubble population with the passage of time were also presented earlier by [Vogt and Balzer \(2005\)](#). Now looking at the distributions on the right in [Fig. 4](#) we can observe a change in characteristics during this duration. The number N indicated on the right top corner of the distribution plot is the number of bubbles detected to get the distribution. This number even in the case of the least number of bubbles (first image) is more than 35,000 and hence should be large enough to be statistically significant. Each plot also shows the mean size (μ) and standard deviation (σ) of the diameter distribution. The mean diameter is seen to reduce monotonically during the initial period while the standard deviation does not change significantly. The nature of the distribution is bi-modal with a second smaller peak towards the higher diameter at the initial time. Eventually the distribution comes close to log-normal. Although not specifically mentioned, in our opinion the earlier work by [Tanaka et al. \(2005\)](#) and [Lee et al. \(2005\)](#) also observed both bimodal and log-normal type distribution in their measurements. In the later part of the results, we will try to explain the reason for these characteristics in the bubble size distribution.

In [Fig. 5](#) we show the result similar to that in [Fig. 4](#) but for a smaller current value of 30 mA (600 mA/cm^2). The results are shown for two times namely, 5 min and 110 min from the starting of electrolysis. The observations of transition of bi-modal to log-normal distributions for bubble sizes made for the 60 mA current is not seen so prominently at 30 mA. The mean sizes presented in [Figs. 4 and 5](#) are summarized in [Fig. 6](#). For 60 mA current two trials are presented which shows that the results are repetitive. At 30 mA current, the mean value of the bubble diameter reduces progressively for an hour and beyond that it reaches a steady state. When the electrolysis process is stopped at the end of the first hour (as in the first trial) and restarted after another hour, the mean diameter shows a sharp increase from the last recorded

value before the electrolysis was stopped. However, with a further progress in time the mean bubble diameter again decreases at an identical rate as before. These results clearly indicate that the bubble size and its distribution on the electrode surface constantly changes for a long time after the starting of the electrolysis process for higher current values. Hence, prescribing a fixed size distribution near the electrode for computing such flows will be correct only if the steady state is reached and this might be a considerable time depending on the value of the current, like an hour for a current value of 60 mA.

Next, we would like to address the reason which might be causing this continuous change in the bubble size. With this view, we present the next set of figures namely [Figs. 7 and 8](#) respectively. Both these figures show the distribution of the number of bubbles in a bubble diameter versus bubble velocity parameter space. The left hand side of both figures show this for initial time ($t=5 \text{ min}$) and the right side show for later time ($t=96 \text{ min}$ and $t=110 \text{ min}$ respectively for [Figs. 7 and 8](#)). If we look at the left side plots we can observe that the smaller diameters have lesser velocities and the bigger ones have higher velocities. In other words, the bubble velocity correlates well with the diameter indicating the predominance of buoyancy force. Similar observations are also presented by [Tanaka et al. \(2005\)](#). However, as we look at the right side of these two figures we observe that the correlation between diameter and velocity breaks down and many small bubbles start acquiring similar rise velocity as that of the large bubbles. This is particularly true for the higher value of current (60 mA). It brings to notice the predominance of factors other than buoyancy in the detachment process of the bubbles. The flow induced by the plume significantly aids the detachment of bubbles from the electrode surface. Similar effect in case of bubble detachment during pool boiling has been discussed in earlier literature ([Zeng et al., 1993](#)). This effect will not be

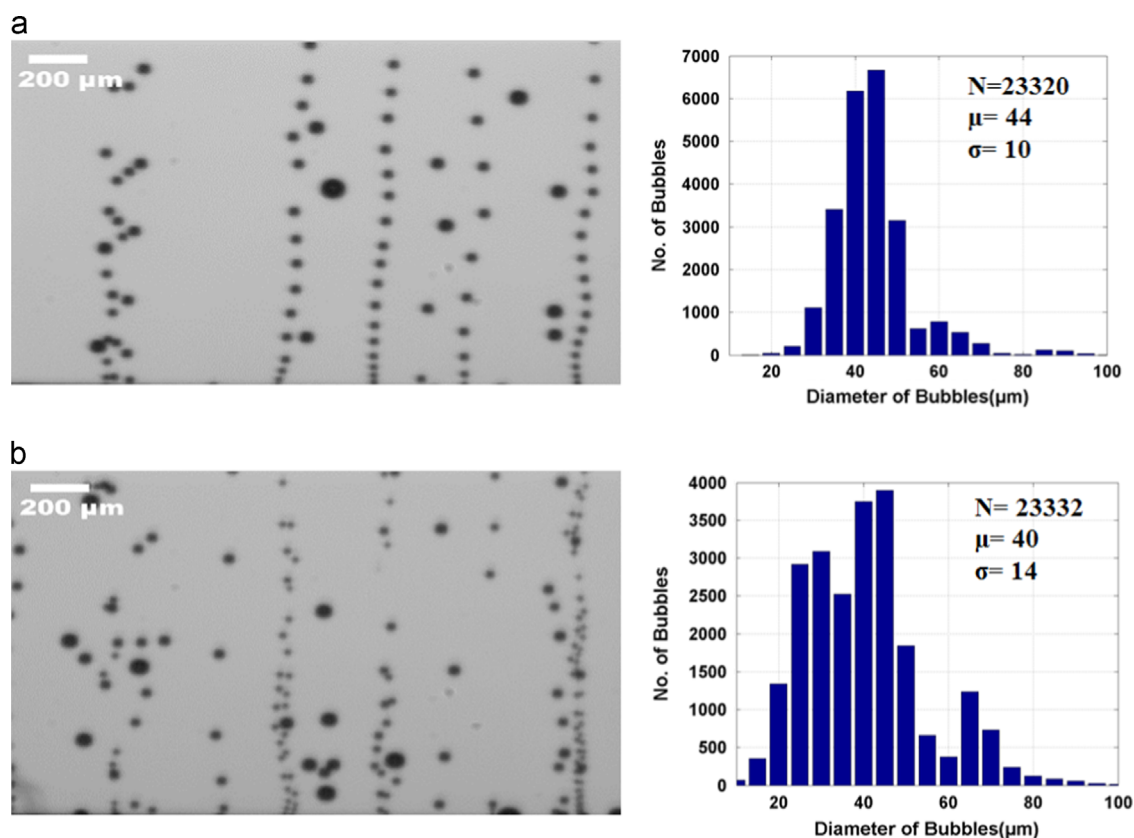


Fig. 5. Bubble size distribution variation at different time period of electrolysis process for current = 30 mA. (a) $t=5 \text{ min}$. (b) $t=110 \text{ min}$.

significant for the case of a single bubble or even for a bubble stream, but the bubbles in a plume are significantly influenced by this effect. The plume develops quite slowly through the two-way coupling between the flows of the entrained liquid and the bubbles. In essence, the induction of the flow by the plume reduces the bubble detachment diameter and this in effect reduces the induced flow. Smaller bubbles, on the other hand, reduces the entrained flow. This competing processes takes some time for the system to reach a steady state. As the reason behind this is fluid

dynamical rather than electrochemical, it is expected that it will be observed for other electrode characteristics as well (Fernandez et al., 2014).

3.2. Bubble growth on the electrode surface

To get further insight into the process we now try to look closely into the process of bubble growth. The first phase of the bubble growth takes place on the surface of the electrode right after it is nucleated at a site. The next phase of the growth happens after the bubble detaches from the electrode surface. In this section, we look at the growth of the bubble on the electrode surface. Fig. 9 shows the sequence of images of the growth of bubble on the electrode surface at a particular site. With the present imaging system it is only possible to capture the bubbles which grow to a higher size, typically above 100 micron. Fig. 10 shows the variation of the diameter of the bubbles on the electrode surface for different nucleation sites at both 30 mA and 60 mA currents. It can be seen from this figure that the attached bubbles grow at a much faster rate for 60 mA as compared to 30 mA. Even for a given current the growth rate is faster for smaller initial diameter. This is typical for the well known diffusion driven growth of the attached bubbles.

The variation of bubble diameter according to simple mass diffusion considerations can be expressed as the equation given as below (Scriven, 1959):

$$R = 2\beta\sqrt{\alpha t}, \quad (1)$$

where R is the bubble radius at an instant t . β is a parameter dependent on the degree of supersaturation and α is the mass diffusivity of the gas in the liquid.

By comparing with the measured growth of the bubbles of different sizes, the value of β for a current value of 30 mA and 60 mA are found to be 0.22 and 0.63 respectively. The higher value of β for higher current is an indicator of the higher degree of supersaturation of water in the vicinity of the electrode. The good representation of the growth rate with Eq. (1) (Scriven, 1959) is in agreement with the constant Fourier number assumption as used in earlier studies (Vogt, 2012; Vogt and Stephan, 2015).

3.3. Bubble growth near the electrode after detachment

The size of a bubble changes not only on the surface but even after detachment. As the bubbles detach from the electrode surface it moves through the supersaturated layer in the vicinity of the electrode. As it moves up through this layer of water supersaturated with hydrogen, its size increases. Fig. 11(a) is an image

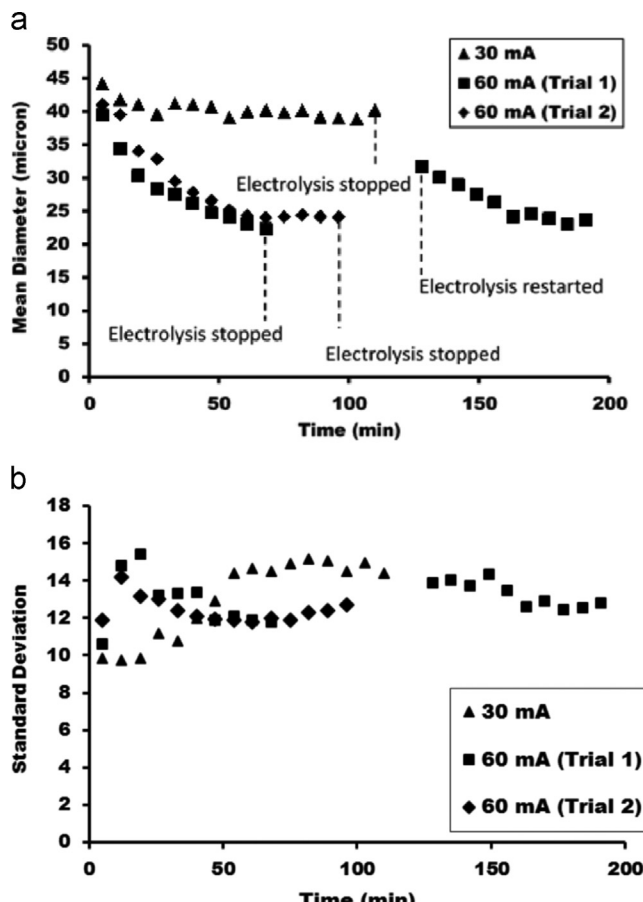


Fig. 6. (a) Variation of the mean bubble size with time for current of 30 and 60 mA during electrolysis. (b) Variation of standard deviation of bubble size with time for the same conditions as above.

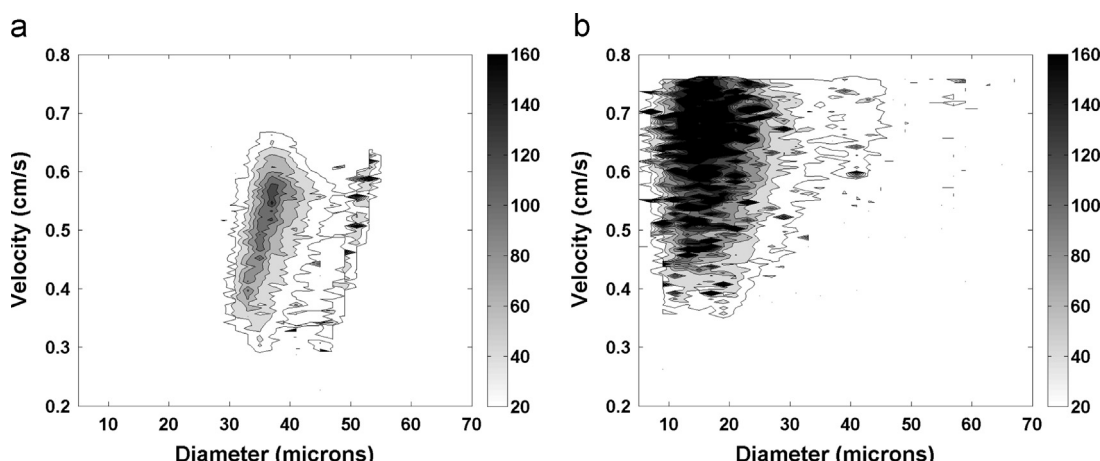


Fig. 7. Distribution of the number of bubbles with its rising velocity and diameter for current=60 mA. (a) $t=5$ min. (b) $t=96$ min.

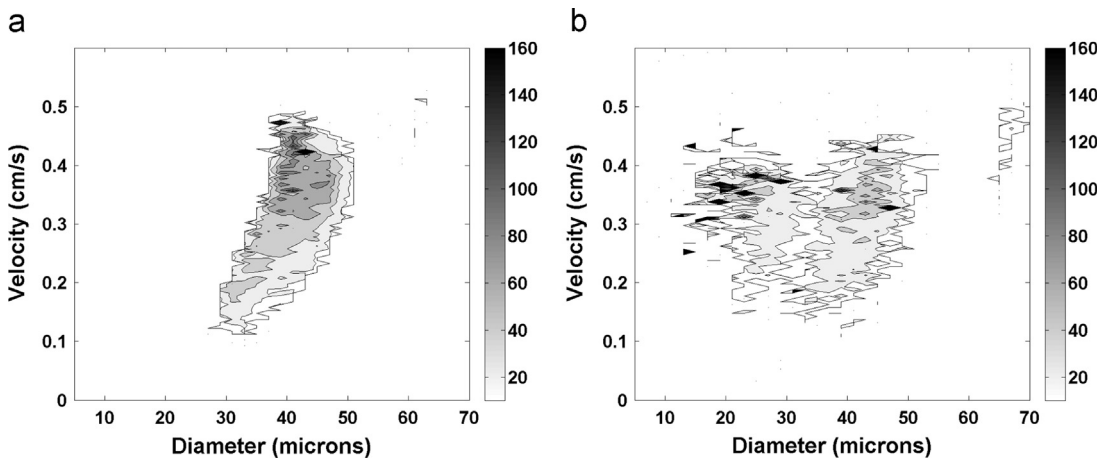


Fig. 8. Distribution of the number of bubbles with its rising velocity and diameter for current = 30 mA. (a) $t=5$ min. (b) $t=110$ min.

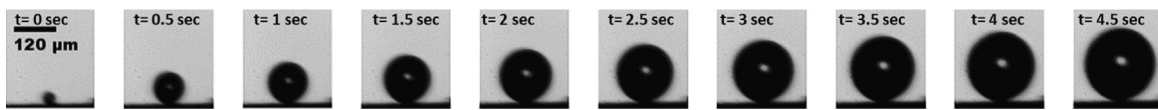


Fig. 9. Sequence of images illustrates bubble growth on electrode surface for 60 mA current.

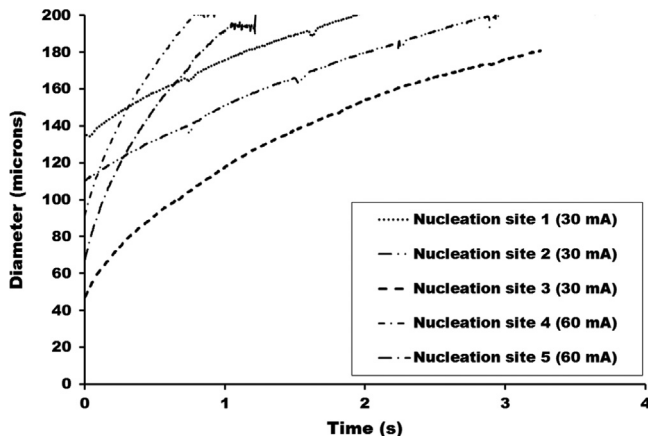


Fig. 10. Temporal variation of diameter of bubble on the electrode surface at different nucleation sites for current values of 30 mA and 60 mA.

showing different streams of bubbles in a plume. Four distinct streams of bubbles at different locations (L1, L2, L3 and L4) are marked in this figure. There are also other streams visible in this image, but, they meander as they interact with the neighbouring streams. It can be noted that the entire plume is a combination of several such individual streams and understanding these streams and their interaction is key to understanding the dynamics of the plume as a whole. Fig. 11(b) shows the variation of diameter along the plume showing clear evidence of bubble growth as bubbles move along the stream. Interestingly, the growth of the bubble is faster in the initial stage followed by a slow growth. Indeed, most of the growth in the stream happens during this initial stage. It could be noted that the current for the above observation is 60 mA. We can see in Fig. 11(c) that the bubble-to-bubble distance (λ) as marked in Fig. 11(a) increases along the bubble stream. This is because a bubble accelerates faster as it grows, this is due to increase in the buoyancy force. It may be noted that although the drag force increases with an increase in bubble diameter, the increase in buoyancy force is proportional to the cube of diameter as opposed to the square of diameter for drag force. Additionally, the drag force in the stream is much less dominant as opposed to a

single bubble rising in the liquid. As the velocities of the bubbles are known from our measurement we can get a very close estimate of the frequency of bubble generation at a particular location. This can be estimated from the ratio of the velocity of the bubble with λ . For the selected streams (L1, L2 and L3 only), the frequency remains fairly constant even if this estimate is made using the local value of velocity and λ at different distances from the electrode surface (Fig. 11(d)). This gives us more confidence in this estimate. When this frequency is plotted with bubble diameter as shown in Fig. 12 at the four different locations, it shows that it inversely correlates with the cube of bubble diameter. This is to say that the rate at which the gas is released at different locations is same for a given current, i.e., $fD^3 = \text{constant}$, where f is the frequency and D the bubble diameter. This has been shown to be true in case of single stream of bubbles (Fernandez et al., 2014) in a recent work. The present observation confirms that this is also true for an individual stream in a plume.

3.4. Influence of bubble growth characteristics on bubble size distribution

Now that we have looked at the bubble growth in individual bubble stream and on the electrode surface we can re-look at the distribution of bubble size. It is evident from the results presented in last sections, that the bubble size is determined from the processes like its nucleation and followed by the diffusion controlled growth. In fact, the later factor plays a very important role in the determination of the size distribution near the electrode surface. We now look at how an initially nucleated bubble grows in the region near to the electrode as per the diffusion controlled growth rate governed by Eq. (1). Fig. 13(a) shows the variation of bubble size with distance from the electrode surface for different initial diameters. In plotting this figure we have made use of velocity of the bubble from Fig. 7(a), i.e., smaller bubbles have lesser velocity and bigger bubbles have higher velocity. So, in effect, the smaller bubbles grow much more near the electrode as the rate of growth is high (see Fig. 10) and it also spends more time near the electrode as it moves slower. Hence, we can expect that the bubbles within a range of diameter will come to very close size within a certain region from the electrode surface. For example, it is shown

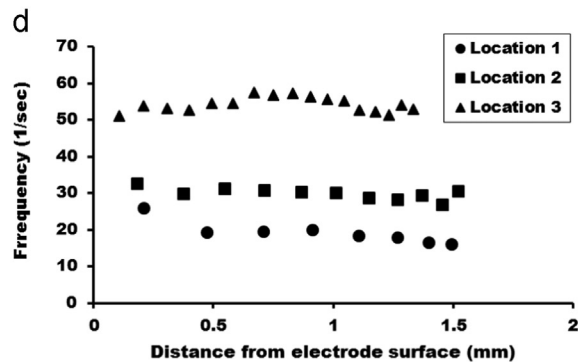
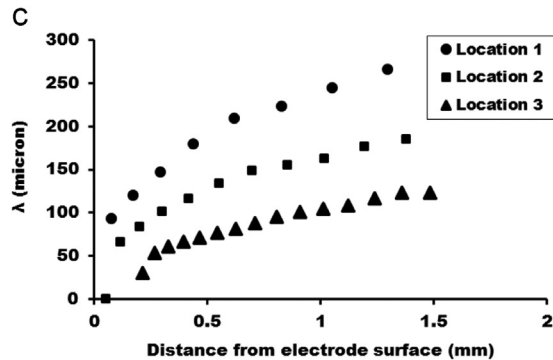
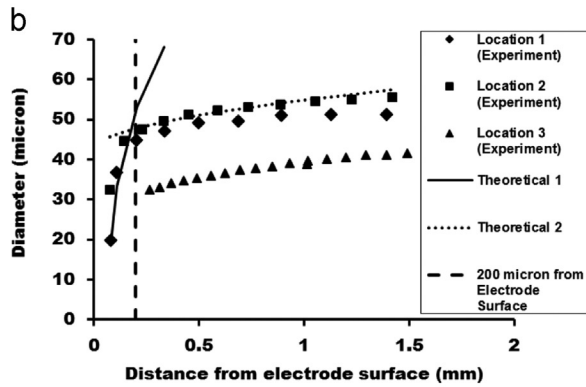
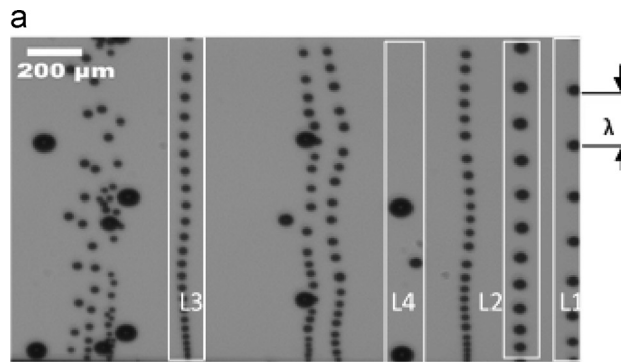


Fig. 11. (a) Image of four different bubble streams in the plume. (b) Variation of bubble diameter along the bubble streams. (c) Temporal variation of bubble spacing (λ) along the bubble streams. (d) Frequency of bubble generation on the electrode surface calculated from the ratio of bubble spacing and local bubble velocity. The current is 60 mA.

in Fig. 13(a) that the bubbles in a range of $40\text{--}100 \mu\text{m}$ come to within $95\text{--}119 \mu\text{m}$ at 1.5 mm from the electrode surface, which is the height of the window in Fig. 4 used for finding the size distribution. Thus there is a clear indication of the bunching of bubble diameter due to the diffusion controlled growth near the electrode surface. The bigger bubbles, however, are least affected by

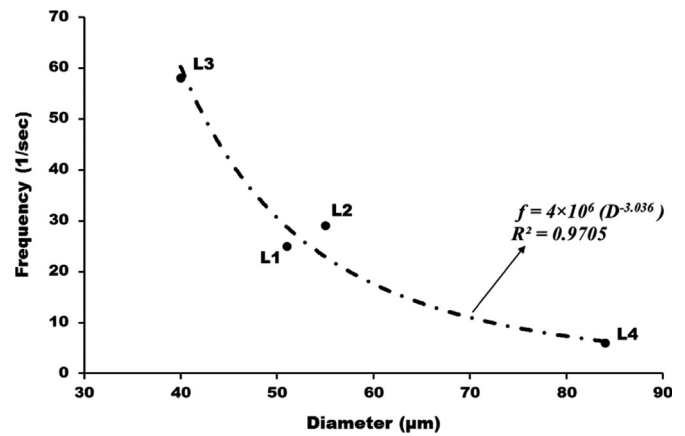


Fig. 12. Variation of frequency of bubble formation with bubble diameter.

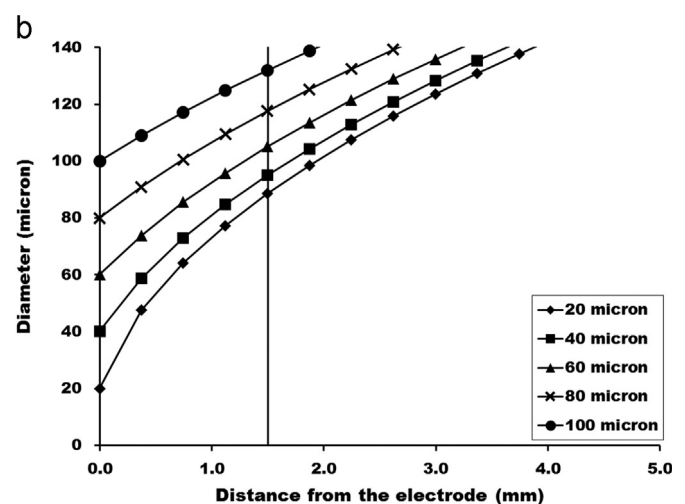
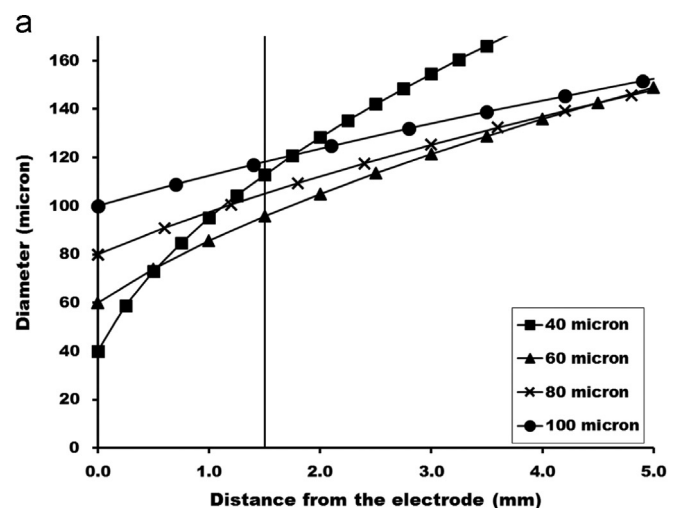


Fig. 13. Theoretical variation (diffusion driven, derived from Eq. (1)) of bubble diameter along the vertical distance from electrode surface with (a) size-dependent bubble velocity (b) constant bubble velocity. The current is 60 mA.

diffusion controlled growth once they detach from the electrode surface. This is schematically represented in Fig. 14, where we can see that the different size bubbles starting from location-I and II comes to similar diameter within a short distance from the electrode. Bigger bubbles, starting from location-III, however hardly grows while passing through the window rapidly. Therefore, we can

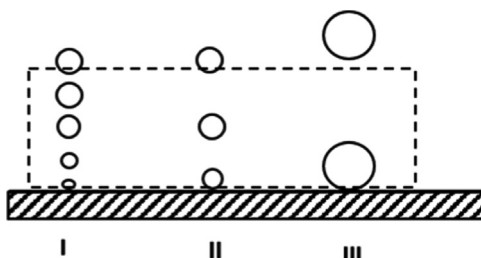


Fig. 14. Schematic of the representation of bubble growth of different sizes in the observation window (dashed line) at initial times.

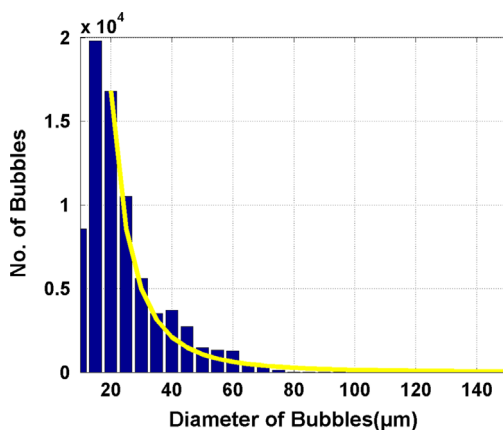


Fig. 15. Bubble size distribution representing the relation between frequency and diameter.

think of two classes in the size distribution, i.e., the one which is affected by the diffusion driven growth after detachment and the bigger bubbles which are not influenced. This could be a reason for our observation of bimodal distribution in the bubble size as observed during the initial phase of electrolysis. At the later stages, the bubble size and velocity correlation breaks down as shown in Fig. 7(b) and thus the smaller bubbles also moves away fast from the electrode surface. This is also observed from the reduction in mean size of the bubbles as the electrolysis process progresses (Fig. 6(a)). Now if we reconstruct the same situation as in Fig. 13(a) but with a constant velocity for all the bubbles (from Fig. 7(b)), we get Fig. 13(b). We can see from Fig. 13(b) that the diameter does not come as close to each other as in Fig. 13(a). Thus the bi-modal distribution is not observed at later stages of electrolysis. At later stage, the distribution is more like a log normal distribution. Although, the detailed reasoning of such a distribution is beyond the scope of this paper but certain general features may be useful to notice here. For example, the frequency of bubble formation as seen from Fig. 11 is related to the inverse cube of the bubble diameter, which explains the lower population of bubbles as the diameter increases.

Fig. 15 shows that the right side of the distribution starting from the maxima can be well represented by an inverse cube variation. It can be noted that there is a reduced population in the smaller bubble size as well which could be due to lesser nucleation of very small bubbles or their coalescence with other bigger or smaller bubbles.

4. Conclusion

The present study brings to attention several important features on bubble characteristics in conjunction with its formation

and transport near the electrode surface. These findings should be useful in improving the effort in capturing several processes in which electrolysis induced bubbles are produced. We observe that the mean bubble size near the electrode reduces constantly as the electrolysis progresses and finally reaches a steady state which takes around an hour for the present conditions. The distribution of bubble size near the electrode is bimodal to begin with and with passage of time it becomes log-normal for higher current densities (1200 mA/cm^2). These effects are not so dominant at relatively lower current densities (600 mA/cm^2). We also show that the flow induced by the plume aids in the detachment of the bubbles and hence the velocity and bubble diameter at later stages of electrolysis does not correlate with each other. This also results in the reduced size of the bubble as the electrolysis process progresses. We see that the diffusive growth of the bubbles is an important process influencing the near-electrode characteristics of the bubble size distribution. The growth of the attached as well as detached bubbles seems to follow diffusion law. It is demonstrated that the growth rate of a bubble can explain certain general features of the bubble size distribution on the electrode surface. This study, it is believed, will help in improving modelling of bubble formation and transport in electrolysis of water relevant to different applications.

Nomenclature

List of Symbols

D:	Bubble diameter
f:	Frequency of bubble formation on the electrode
N:	Number of bubbles used for finding the distribution
R:	Radius of the bubble
t:	Time
α :	Mass diffusivity of gas
β :	Growth constant (Scriven, 1959)
λ :	Bubble-to-Bubble distance in a stream
μ :	Mean of the bubble size distribution
σ :	Standard deviation of the bubble size distribution

Acknowledgements

Partial financial support of the Naval Research Board (India) (Grant no. DNRD/05/4003/NRB/224) is gratefully acknowledged.

References

- Charton, S., Janvier, J., Rivalier, P., Chaînet, E., Caire, J.-P., 2010. Hybrid sulfur cycle for H_2 production: a sensitivity study of the electrolysis step in a filter-press cell. *Int. J. Hydrom. Energy* 35 (4), 1537–1547.
- Fernandez, D., Maurer, P., Coey, J., Martine, M., Mobius, M.E., 2014. Bubble formation at a gas-evolving microelectrode. *Langmuir* 30 (43), 13065–13074.
- Janssen, L.J.J., Hoogland, J.G., 1970. The effect of electrolytically evolved gas bubbles on the thickness of the diffusion layer. *Electrochim. Acta* 15, 1013–1023.
- Janssen, L.J.J., Hoogland, J.G., 1973. The effect of electrolytically evolved gas bubbles on the thickness of the diffusion layer-ii. *Electrochim. Acta* 18, 543–550.
- Jomard, F., Feraud, J.-P., Morandini, J., Couvat, Y.D.T., Caire, J.-P., 2008. Hydrogen filter press electrolyser modelled by coupling fluent and flux expert codes. *J. Appl. Electrochem.* 38 (3), 297–308.
- Khosla, N., Venkatachalam, S., Somasundaran, P., 1991. Pulsed electrogeneration of bubbles for electroflootation. *J. Appl. Electrochem.* 21 (11), 986–990.
- Kikuchi, K., Tanaka, Y., Sahara, Y., Maeda, M., Kawamura, M., Ogumi, Z., 2006. Concentration of hydrogen nanobubbles in electrolyzed water. *J. Coll. Interface Sci.* 298 (2), 914–919.
- Lee, S., Sutomo, W., Liu, C., Loth, E., 2005. Micro-fabricated electrolytic micro-bubbler. *Int. J. Multiph. Flow* 31 (6), 706–722.
- Murai, Y., Matsumoto, Y., 2000. Numerical study of the three-dimensional structure of a bubble plume. *J. Fluids Eng.* 122 (4), 754–760.

- Nierhaus, T., van Parys, H., Dehaeck, S., van Beeck, J., Deconinck, H., Deconinck, J., Hubin, A., 2009. Simulation of the two-phase flow hydrodynamics in an irde reactor. *J. Electrochem. Soc.* 156 (9), 139–148.
- Plowman, B.J., Jones, L.A., Bhargava, S.K., 2015. Building with bubbles: the formation of high surface area honeycomb-like films via hydrogen bubble templated electrodeposition. *Chem. Commun.* 51 (21), 4331–4346.
- Scriven, L., 1959. On the dynamics of phase growth. *Chem. Eng. Sci.* 10 (1–2), 1–13.
- Tanaka, Y., Kikuchi, K., Sahara, Y., Ogumi, Z., 2005. Bubble visualization and electrolyte dependency of dissolving hydrogen in electrolyzed water using solid-polymer-electrolyte. *Electrochim. Acta* 50 (25), 5229–5236.
- Vogt, H., 2012. The actual current density of gas-evolving electrodes—notes on the bubble coverage. *Electrochim. Acta* 78, 183–187.
- Vogt, H., Balzer, R., 2005. The bubble coverage of gas-evolving electrodes in stagnant electrolytes. *Electrochim. Acta* 50 (10), 2073–2079.
- Vogt, H., Stephan, K., 2015. Local microprocesses at gas-evolving electrodes and their influence on mass transfer. *Electrochim. Acta* 155, 348–356.
- Wang, Y., Zheng, Y., Xu, X., Dubuisson, E., Bao, Q., Lu, J., Loh, K.P., 2011. Electrochemical delamination of cvd-grown graphene film: toward the recyclable use of copper catalyst. *ACS Nano* 5 (12), 9927–9933.
- Westerheide, D.E., Westwater, J., 1961. Isothermal growth of hydrogen bubbles during electrolysis. *AIChE J.* 7 (3), 357–362.
- Zeng, K., Zhang, D., 2010. Recent progress in alkaline water electrolysis for hydrogen production and applications. *Progr. Energy Combust. Sci.* 36 (3), 307–326.
- Zeng, L., Klausner, J., Mei, R., 1993. A unified model for the prediction of bubble detachment diameters in boiling systems—I. Pool boiling. *Int. J. Heat Mass Transf.* 36 (9), 2261–2270.